Influence of the quantum confined Stark effect on photoluminescence spectra of PbTe nanodots embedded in a CdTe matrix

R. Leitsmann* and F. Bechstedt

European Theoretical Spectroscopy Facility (ETSF) and Institut für Festkörpertheorie und -optik, Friedrich-Schiller-Universität Jena, Max-Wien-Platz 1, 07743 Jena, Germany

(Received 12 July 2009; revised manuscript received 9 September 2009; published 5 October 2009)

The quantum confined Stark effect induced by electric fields is of outstanding importance for nanostructure properties. In embedded quantum dots, it occurs as consequence of internal electric fields related to interface charges. A quantum dot model including the quantum confined Stark effect is proposed. It is applied to PbTe/CdTe quantum dot precipitates. The predicted photoluminescence spectra are compared with results of photoluminescence experiments. The unexpected photoluminescence intensity drop at low temperatures is interpreted to be a consequence of the internal quantum confined Stark effect.

DOI: 10.1103/PhysRevB.80.165402 PACS number(s): 68.35.Ct, 68.65.Hb, 73.22.−f, 73.21.La

I. INTRODUCTION

The quantum confined Stark effect (QCSE) is well-known for semiconductor nanostructures, especially for quantum-well structures.[1] It can be induced by external fields but it also occurs due to internal electric fields. This renders the QCSE a versatile mechanism for designing new optoelectronic applications. For quantum-dot structures, it has been studied in the presence of external and strain-induced internal electric fields.[2,3] However, also in unbiased and unstrained embedded nanocrystals, the QCSE has recently been predicted as a direct consequence of polar dot-matrix interfaces.[4] In such structures with alternating cation(A)- and anion(B)-terminated interfaces, interface charges and electric polarization fields influence electronic states, interface thickness, actual atomic positions, and electrostatic fields.[5–7] The mirror symmetry is usually broken and the locally built-in electric field tends to spatially separate the center of gravity for electrons and holes, i.e., it yields an internal QCSE.[4] The consequence of this effect on optical properties have been discussed only in a qualitative manner so far. In this work, we present an almost analytical model, which is able to include the effect of internal electric fields, the level quantization, and the temperature-dependent level occupation into the calculation of optical spectra such as luminescence spectra.

Recently, strong progress in the generation of high-quality lead-salt quantum dots (QDs) has been made. Beside colloidal QDs,[8–11] also PbTe QDs embedded in a CdTe matrix could be fabricated.[12,13] The latter ones are of particular interest for gas sensing applications in the mid-infrared (MIR) range and will be considered as model systems for the occurrence of internal electric fields. The fabrication approach is based on an epitaxial precipitation of lattice-type mismatched heterostructures.[12] Despite an almost vanishing lattice-constant mismatch (average theoretical lattice-constant a_0=6.41 Å) and the same fcc Bravais lattice, the compounds PbTe and CdTe exhibit a different crystal structure. They crystallize in rocksalt (rs) and zinc blende (zb) structures, respectively. The fabrication approach yields wetting-layer-free QDs with highly symmetric shapes[12,13] and atomically sharp heterointerfaces.[5,6,13] Furthermore, these QDs are defect free and exhibit an intense continuous-wave cw photoluminescence (PL) at room temperature.[12,13] However, at low temperatures, an unexpected PL intensity drop has been observed. As possible explanations for this effect, Schwarzl *et al.* could rule out a splitting of the ground state into a "dark" and a "bright" state or a type I to type II band alignment.[14] Other possible mechanisms to explain this effect are a thermal redistribution of charge carriers or the appearance of an internal QCSE, as we will show in this article.

The dot sizes and the vertical positions of the dots can be controlled by the growth conditions.[15] The fabrication starts with molecular beam epitaxy (MBE) growth of a two-dimensional PbTe layer (E_{gap}=320 meV at 300 K)[16] with a thickness in the nanometer range sandwiched between CdTe barrier layers (E_{gap}=1.53 eV).[17] This PbTe quantum well is subsequently transformed into QDs by thermal annealing, based on the immiscibility of the two materials[18] and the minimization of the interface energy.[6] The resulting thermodynamic equilibrium crystal shape, a truncated rhombo-cubo-octahedron with A- and B-terminated facets on opposite sides, is experimentally well established by high resolution cross-sectional transmission electron microscopy (HRXTEM) studies.[5] Detailed images of the staring PbTe/CdTe quantum-well structure and the resulting embedded PbTe QDs are given in Figs. 1(a) and 1(b) of Ref. 19, respectively. It exhibits a C_{3v} symmetry with the symmetry axis along [111]. The symmetry reduction in the original O_h (rs) and T_d (zb) point groups is related to the inequality of oppositely terminated but pairwise occurring dot-matrix interfaces as shown in Fig. 1(b). Using a notation based on zb-CdTe (Ref. 6) we find A-terminated dot-matrix interfaces at the $(\bar{1}00)$, $(0\bar{1}0)$, $(00\bar{1})$, (111), $(1\bar{1}\bar{1})$, $(\bar{1}\bar{1}1)$, $(\bar{1}1\bar{1})$ facets and B-terminated dot-matrix interfaces at the (100), (010), (001), $(\bar{1}\bar{1}\bar{1})$, $(\bar{1}11)$, $(11\bar{1})$, $(1\bar{1}1)$ facets. Interestingly, these facet orientations lead to a dominance of cation-terminated facets at the $[\bar{1}\bar{1}\bar{1}]$ half of the nanocrystallites and vice versa of anion-terminated facets at the [111] half[4] as visible in Fig. 1(b). The resulting interface distribution yields a symmetry break. Since A (B)-terminated interfaces exhibit positive (negative) interface charges a strong internal (even inhomogeneous) electrostatic field is induced with the principal axis along the [111] direction.[4] Such an electrostatic field signifi-

 ©2009 The American Physical Society

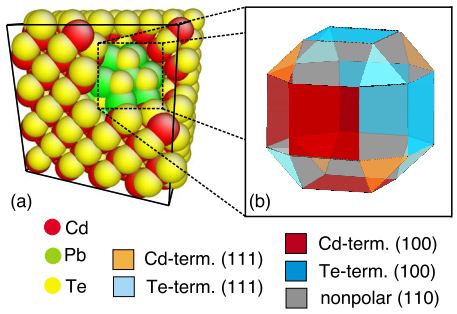

FIG. 1. (Color online) (a) Model of a PbTe QD embedded in CdTe matrix. To enhance the visibility in the first quadrant no matrix atoms are shown. (b) Schematic representation of the occurring dot-matrix interface facets. Different terminations are indicated by different colors.

cantly influences the electronic properties of the nanocrystallite system. The field influence on the distribution of the highest occupied NC orbital (HONO) as well as of the lowest unoccupied NC orbital (LUNO) is demonstrated in Fig. 2. As a consequence of the strong electric field the maxima of the probability to find a hole or an electron are spatially well separated by the distance Δ_{wav}. Additionally the internal QCSE decreases the energy separation of the HONO-LUNO level difference $E_{\mathrm{gap}}+E_{\mathrm{conf}}$ by a Stark shift Δ_{Stark}. Thereby, $E_{\mathrm{gap}}(E_{\mathrm{conf}})$ denotes the bulk gap (the sum of the lowest confinement energies of electrons and holes).

II. POTENTIAL WELL MODEL

The influence of spatial quantization and the QCSE on the PL spectra of NCs is modeled using a three-dimensional (3D) parabolic potential well and a homogeneous electric field in x direction (parallel to the [111] axis) for each carrier type

$$H = -\frac{\hbar^2 \nabla_{\mathbf{r}}^2}{2m^*} + \alpha \mathbf{r}^2 + Fx, \tag{1}$$

where m^* is either the effective electron mass m_e^* or the effective hole mass m_h^*, F represents the strength of the electric

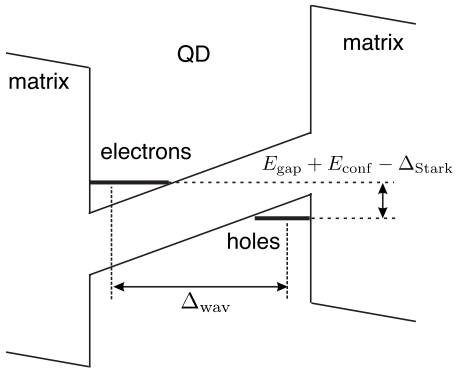

FIG. 2. Schematic confinement potential of an embedded QD with internal electric field. The lowest electron and hole levels are indicated by horizontal solid lines. The spatial separation Δ_{wav} of the maxima between the HONO and LUNO probability distributions and the energy shift Δ_{Stark} due to the field-induced potential are indicated.

field induced by the interfaces, and the parameter α which is related to the QD size will be fixed later on. In order to reduce the number of adjustable parameters, we assume equal confinement potentials for electrons and holes. Thereby we define the effective masses as average of the transversal and longitudinal masses $m^* = \sqrt{(m_t^*)^2 m_l^*}$ as proposed in Ref. 14. The parabolic shape of the confinement potential for electrons and holes has two main advantages. First, the dependence of the so-called confinement energy E_{conf}, which is defined as the difference of the QD ground-state energy level difference between electrons and holes and the corresponding bulk band gap, on the QD size D_{QD} is (at least for small QD systems) better described using 3D parabolic potentials.[20] Apart from PbTe QDs, also for Si nanocrystals either hydrogenated or embedded in a SiO_2 matrix a diameter dependence D_{QD}^{-n} of the confinement energy E_{conf} with a power n somewhat below 1 has been found,[21,22] in contrast to the prediction $n=2$ assuming one-dimensional or 3D (spherical) rectangular potential wells. Second, the parabolic potential well model can be solved analytically even in the presence of an electric field F, which simply yields a displacement of the parabola origins against each other describing the spatial separation of the electron and hole wave functions

$$\Delta_{\mathrm{wav}} = \frac{F}{\alpha} \tag{2}$$

and the energy shift

$$\Delta_{\mathrm{Stark}} = \frac{F^2}{2\alpha}. \tag{3}$$

Equation (2) is used to define the QD diameter D_{QD} via the parameter α. For this purpose, we have calculated the spatial separation of the electron and hole wave functions in a reference system with $D_{\mathrm{QD}}^{\mathrm{ref}}=12$ Å, using *ab initio* techniques.[4] Evaluating the electrostatic potential in this system we determined the strength of the internal electric field F^{ref} to ≈ 0.01 eV/Å and $\Delta_{\mathrm{wav}}^{\mathrm{ref}}$ to $0.7 D_{\mathrm{QD}}^{\mathrm{ref}}$. The parameter α is thereby given by[20]

$$\alpha = \frac{F}{\Delta_{\mathrm{wav}}} = \frac{F}{0.7 D_{\mathrm{QD}}} = \frac{F^{\mathrm{ref}} D_{\mathrm{QD}}^{\mathrm{ref}}}{0.7 (D_{\mathrm{QD}})^2}. \tag{4}$$

The resulting electronic energy levels allow to define the optical transition energies of such a model system

$$E_{\mathrm{trans}}^{cv} = \varepsilon_c + \varepsilon_v + E_{\mathrm{gap}} - \Delta_{\mathrm{Stark}}, \tag{5}$$

where ε_c and $\varepsilon_v (c,v=0,1,2,\ldots,)$ are the electron and hole eigenvalues of the Hamiltonian (1) with $E_{\mathrm{conf}}=\epsilon_c+\epsilon_v$ for the lowest levels $c=0$ and $v=0$. To describe the temperature dependence of the PL signal it is essential to include, beside the temperature dependence of the bulk PbTe band gap $E_{\mathrm{gap}}=E_{\mathrm{gap}}(T)$, also the strain influence $\Delta^{\mathrm{Strain}}(T)$ induced by the different thermal expansion coefficients β of PbTe (19.8×10^{-6}/K at 300 K) and the matrix material CdTe

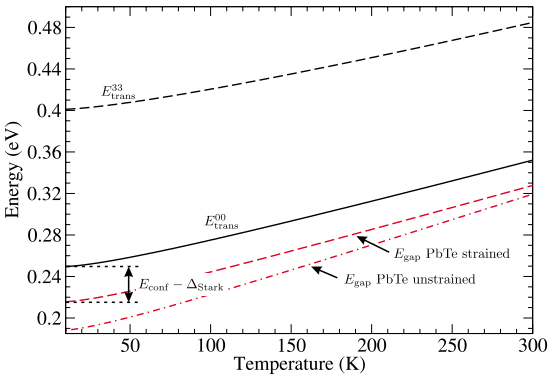

FIG. 3. (Color online) Electron-hole transition energies for a 29-nm PbTe/CdTe QD as function of temperature. The black solid line depicts the calculated ground-state transition energy E^{00}_{trans}, while the excited-state transition energy E^{33}_{trans} is given as black dashed line. The red lines represent the unstrained (dash-dotted line) and strained (dashed line) bulk PbTe band gap.

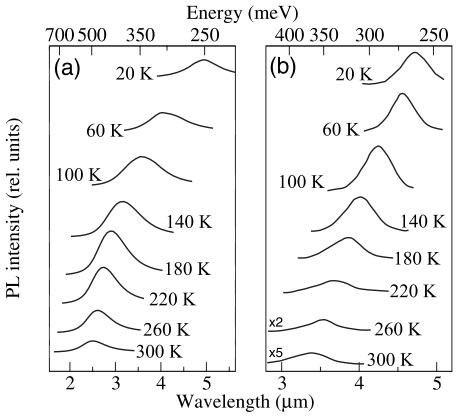

FIG. 4. Temperature-dependent PL spectra:(a) Theoretical prediction for a 29-nm PbTe QD; (b) Experimental observation for PbTe/CdTe QDs formed from an initially 5-nm-thick PbTe layer—taken from Schwarzl *et al.* (Ref. 14).

$(4.9\times10^{-6}/\mathrm{K}$ at 300 K).[14] This leads to the following temperature-dependent band gap of strained PbTe

$$E_{gap}(T) = E_{gap}(0) + \frac{aT^2}{(T+b)} + \Delta_{Strain}(T). \tag{6}$$

In the explicit calculations, we use a PbTe zero temperature band gap of $E_{gap}(0)=0.187$ eV (Ref. 23) and the parameters $a=5\cdot10^{-4}$ eV/K and $b=40$ K.[24] The strain influence $\Delta_{Strain}(T)$ is modeled via

$$\Delta_{Strain}(T) = \frac{\partial E_{gap}}{\partial p} P(T) \tag{7}$$

with the hydrostatic pressure coefficient $\frac{\partial E_{gap}}{\partial p}=-75$ meV/GPa for PbTe (Ref. 25), which we assume to be constant with respect to the temperature T. The contact pressure $P(T)$ is calculated using the parameters given by Schwarzl *et al.*[14] Additionally the effective masses m^*_e and m^*_h of PbTe decrease with temperature due to the decreasing band gap (e.g., $m^*_{e,t}(300K)=0.031m_0$, $m^*_{e,t}(80K)=0.024m_0$, $m^*_{h,t}(300K)=0.036m_0$, and $m^*_{h,t}(80K)=0.027m_0$). To model this, we have used the scheme of Preier.[26] As a consequence, the quantum confinement for both types of carriers will strongly increase with decreasing temperature, i.e., $E_{conf}=\epsilon_{c=0}+\epsilon_{v=0}$ increases with decreasing temperature. This can be seen in Fig. 3, where we have exemplarily plotted the temperature dependence of E_{gap} (6), E^{00}_{trans} (5), and E^{33}_{trans} (5) for a 29-nm PbTe QD.

III. PHOTOLUMINESCENCE SPECTRA

The spectral distribution and the intensity of the PL signal can be calculated by means of an expression similar to the frequency-dependent dielectric function $\varepsilon(\omega,T)$ but with modified occupation numbers containing the nonequilibrium electron and hole Fermi functions f_e and f_h with quasi-Fermi energies for both particle types, via[27]

$$I^{PL}(\omega,T) \sim \left[\frac{f_e(1-f_h)}{f_h-f_e}\right] \mathrm{Im}[\varepsilon(\omega,T)]. \tag{8}$$

Using the independent-particle approximation for the dielectric function[28] and approximating the size dependence of the transition matrix elements by the overlap integrals of the corresponding electron on hole wave functions one obtains

$$I^{PL}(\omega,T) = C\sum_{c,v} \frac{f_e(\hbar\omega-\epsilon_v)[1-f_h(\epsilon_v)]}{[\epsilon_c+\epsilon_v+E_{gap}-\Delta_{Stark}]^2} \times \frac{|\langle c|v\rangle|^2\Gamma(T)e^{-T/T_0}}{(\epsilon_c+\epsilon_v+E_{gap}-\Delta_{Stark}-\hbar\omega)^2+\Gamma(T)^2}, \tag{9}$$

where we have introduced an additional temperature-dependent broadening function $\Gamma(T)$ (Ref. 20) and a damping term e^{-T/T_0}. The first term qualitatively models two important broadening mechanisms: the lifetime broadening of electrons and holes due the scattering of acoustic or LO phonons and the line broadening due to the size distribution of the investigated QDs. The second damping term e^{-T/T_0} describes phenomenologically the decay of the PL intensity at high temperatures due to nonradiative recombination processes. Their strength is characterized by a critical temperature T_0. Such a decay behavior has been explicitly observed for the PL signal of a-Si:H (Ref. 29) and chalcogenide glasses.[30] Typical critical temperatures for a-Si:H are in the range of 10 to 20 K,[29] which compare quite well with the parameter $T_0=33$ K used in this work to model the nanocrystalline telluride systems. The overlap integrals of electron and hole wave functions $\langle c|v\rangle$ are evaluated using the three-dimensional oscillator eigenfunctions of the Hamiltonian (1) up to $c,v=5$. Altogether using the 3D oscillator model, we are able to calculate the temperature- and frequency-dependent PL spectra of embedded PbTe QDs taking into account the internal QCSE by means of expression (9). Results for the frequency-dependent PL spectra of a 29-nm QD are illustrated in Fig. 4(a) for different temperatures. The obtained results are in qualitative agreement with the experimentally observed cw-PL spectra [Fig. 4(b)] of PbTe QDs originating from an initially 5-nm-

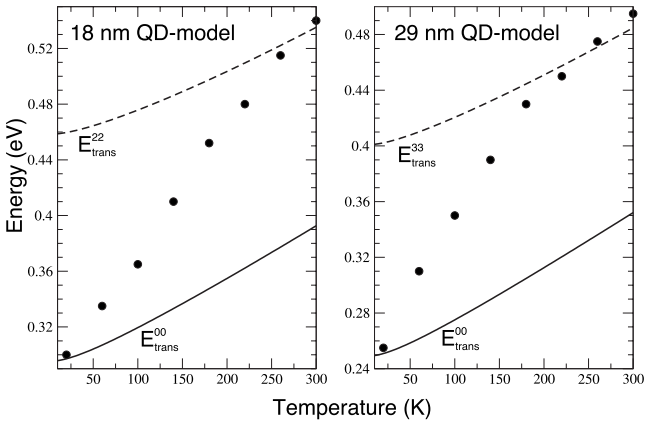

FIG. 5. Theoretical (black dots) peak energies of PL emission spectra of PbTe/CdTe QDs as function of temperature. The full and dashed lines depict calculated ground-state and excited-state transition energies, respectively.

thick PbTe layer.[14] The in this way estimated QD diameter of 29 nm for QD samples with an initial 5-nm PbTe layer is in good agreement with the QD size distribution found by TEM.[15]

From the PL spectra in Fig. 4, we extract the maximum PL peak position E_{PL}. In Fig. 5 these maxima positions are plotted versus temperature. At low temperatures, they match the ground-state transition energy E^{00}_{trans}, while at larger temperatures they approach toward the excited-state transition E^{22}_{trans} (18-nm QD) or E^{33}_{trans} (29-nm QD).

The significantly stronger temperature dependence of the predicted peak energy of the PL emission spectra in comparison with that of a certain transition energy E^{cv}_{trans} with fixed values c,v is a consequence of the temperature dependence of the electron and hole level occupation numbers. With increasing temperature more and more excited quantized states will be populated by electrons or holes. In addition, the overlap integrals of such states are much larger than for the ground state, because they are less influenced by the QCSE. Consequently at higher temperatures mainly excited states will contribute to the PL signal and lead to a temperature-dependent blue shift in the spectra $\Delta_{\mathrm{ex}}(T)$, so that we observe the PL peaks at positions

$$E_{\mathrm{PL}}(T) = E^{00}_{\mathrm{trans}}(T) + \Delta_{\mathrm{ex}}(T) = E_{\mathrm{gap}}(T) + E_{\mathrm{conf}} - \Delta_{\mathrm{Stark}} + \Delta_{\mathrm{ex}}(T). \tag{10}$$

In Fig. 5, in both cases of QD diameters, a nonvanishing blue shift $\Delta_{\mathrm{ex}}(T)$ of the PL peak position compared to ground-state transition E^{00}_{trans} is clearly observed. This again indicates the involvement of excited-state contributions in the observed PL spectra.

The temperature-dependence of the integrated PL intensities can be obtained by a simple energy integration of Eq. (9).

$$I^{\mathrm{PL}}_{\mathrm{int}}(T) = \int_0^\infty d\omega I^{\mathrm{PL}}(\omega, T), \tag{11}$$

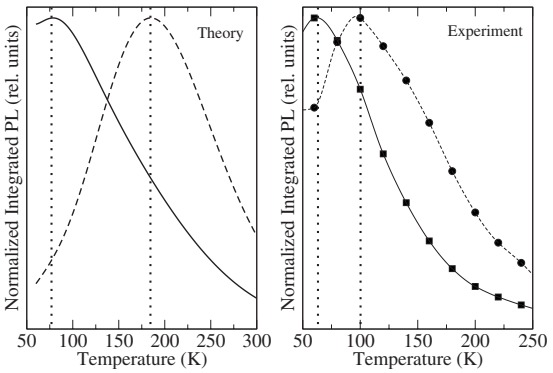

FIG. 6. Normalized integrated PL intensity. Left panel: theoretical prediction for a 18-nm QD (solid line) and a 29-nm QD (dashed line). Right panel: experimental data of optimum annealed 3-nm (squares) and 5-nm (circles) PbTe/CdTe samples. Vertical dotted lines indicate the maxima

$$I^{\mathrm{PL}}_{\mathrm{int}}(T) = \tilde{C}\sum_{c,v} \frac{f_e(\epsilon_c + E_{\mathrm{gap}}(T) - \Delta_{\mathrm{Stark}})}{[\epsilon_c + \epsilon_v + E_{\mathrm{gap}} - \Delta_{\mathrm{Stark}}]^2}[1 - f_h(\epsilon_v)] \times |\langle c|v\rangle|^2 e^{-T/T_0}. \tag{12}$$

In Fig. 6, the integrated PL intensities of our theoretical model are compared with the integrated PL intensity measured for PbTe QD samples with initially 3-nm and 5-nm layer thickness. In both cases, the PL intensity increases at first until a certain temperature is reached above which the PL intensity decreases considerably. The temperature of the experimental maximum PL output is about 55 (100) K for the 3 (5)-nm sample, which compares quite well with the theoretical prediction of 75 (180) K for 18 (29) nm PbTe QDs. Due to the size distribution in the samples studied experimentally the quantitative comparison is difficult. For instance the predicted PL maxima of the 29-nm QD compares much better with the high temperature shoulder of the 5-nm sample at about 150 K.

The observed low-temperature behavior, especially the drop down of the PL intensity after reaching a maximum in Fig. 6, is in contrast to what has been observed for the most zb-based III-V QDs for which the PL intensity is constant in this temperature range. The discrepancy can be traced back to the appearance of the internal QCSE in embedded PbTe QDs. Two main mechanisms of the field influence have been stated. In particular, the spatial separation of the HONO and LUNO states leads to reduced optical transition matrix elements. For very low temperatures for which mainly the ground-state electron and hole levels $c=0$ and $v=0$ are occupied this reduction gives rise to a reduced PL intensity. At higher temperatures also excited states will contribute considerably to the PL signal (see Fig. 5). However, these states are less influenced by the QCSE and exhibit larger transition matrix elements, which leads to an increased PL intensity. At even higher temperatures, in addition to other loss mechanisms, the thermal escape of carriers out of the QDs reduces the PL signal again.[31–33] Our model also explains the QD size influence. With increasing QD diameter the electron-hole separation increases as well. Therefore, in larger QDs,

higher lying excited states have to be populated to reach a sufficient wave function overlap. This leads to the observed shift in the integrated PL maxima to higher energies with increasing QD diameter.

IV. SUMMARY

We have proposed a QD confinement model which describes the sizes dependence of the confinement energy for small QDs better than the commonly used models. Furthermore, this model is able to treat eventually occurring internal electric fields. In particular, the QCSE can be taken into account. Using this model, we are able to explain the temperature dependence of PL spectra of embedded semiconductor QD with polar interfaces. As prototypical systems, we have studied PbTe QDs embedded in CdTe layers for which we could demonstrate the influence of the internal QCSE by the characteristic temperature and QD size dependence of the PL intensity. In particular, we have given one explanation for the observed low-temperature drop down of the integrated PL intensity.

ACKNOWLEDGMENTS

We acknowledge valuable discussions with J. Furthmüller and F. Fuchs. In addition we thank W. Heiss from the Institut für Halbleiter und Festkörperphysik of the Johannes-Keppler-Universität Linz, Austria for his comments and suggestions. The work was financially supported by the Fonds zur Förderung der Wissenschaftlichen Forschung (Austria) in the framework of SFB25, Nanostrukturen für Infrarot-Photonik (IR-ON) and the EU via the I3 project ETSF (GA No. 211956). Grants of computer time from the Höchstleistungsrechenzentrum Stuttgart and Munich are gratefully acknowledged.

*roman@ifto.physik.uni-jena.de

[1] Y.-H. Kuo, Y. K. Lee, Y. Ge, S. Ren, J. E. Roth, T. I. Kamins, D. A. B. Miller, and J. S. Harris, Nature (London) **437**, 1334 (2005).
[2] S. A. Empedocles and M. Bawendi, Science **278**, 2114 (1997).
[3] M. Gurioli and S. Sanguinetti, Appl. Phys. Lett. **78**, 931 (2001).
[4] R. Leitsmann and F. Bechstedt, Phys. Rev. B **78**, 205324 (2008).
[5] R. Leitsmann, L. E. Ramos, F. Bechstedt, H. Groiss, F. Schäffler, W. Heiss, K. Koike, H. Harada, and M. Yano, New J. Phys. **8**, 317 (2006).
[6] R. Leitsmann, L. E. Ramos, and F. Bechstedt, Phys. Rev. B **74**, 085309 (2006).
[7] R. Leitsmann and F. Bechstedt, Phys. Rev. B **76**, 125315 (2007).
[8] R. Espiau de Lamaestre, H. Bernas, D. Pacifici, G. Franzo, and F. Priolo, Appl. Phys. Lett. **88**, 181115 (2006).
[9] M. V. Kovalenko, D. V. Talapin, M. A. Loi, F. Cordella, G. Hesser, M. I. Bodnarchuk, and W. Heiss, Angew. Chem., Int. Ed. **47**, 3029 (2008).
[10] J. J. Urban, D. V. Talapin, E. V. Shevchenko, C. R. Kagan1, and C. B. Murray, Nature Mater. **6**, 115 (2007).
[11] M. Fernee, A. Watt, J. Warner, J. Riches, N. Heckenberg, and H. Rubinsztein-Dunlop, J. Cryst. Growth **270**, 380 (2004).
[12] W. Heiss, H. Groiss, E. Kaufmann, M. Böberl, G. Springholz, F. Schäffler, K. Koike, H. Harada, and M. Yano, Appl. Phys. Lett. **88**, 192109 (2006).
[13] W. Heiss *et al.*, J. Appl. Phys. **101**, 081723 (2007).
[14] T. Schwarzl, E. Kaufmann, G. Springholz, K. Koike, T. Hotei, M. Yano, and W. Heiss, Phys. Rev. B **78**, 165320 (2008).
[15] H. Groiss *et al.*, Appl. Phys. Lett. **91**, 222106 (2007).
[16] S. Yuan, H. Krenn, G. Springholz, Y. Ueta, G. Bauer, and P. J. McCann, Phys. Rev. B **55**, 4607 (1997).
[17] G. Nimtz, I. Broser, and M. Rosenzweig, *Numerical Data and Functional Relationships in Science and Technology*, Landolt-Börnstein, Vol. 17/b (Springer, Berlin, 1982).
[18] V. Leute and R. Schmidt, Z. Phys. Chem. **172**, 81 (1991).
[19] H. Groiss, G. Hesser, W. Heiss, F. Schäffler, R. Leitsmann, F. Bechstedt, K. Koike, and M. Yano, Phys. Rev. B **79**, 235331 (2009).
[20] R. Leitsmann, *Hetero-und Nanostrukturen ionischer Materialien* (Südwestdeutscher Verlag für Hochschulschriften, Saarbrücken, 2009).
[21] H.-C. Weissker, J. Furthmüller, and F. Bechstedt, Phys. Rev. B **65**, 155328 (2002).
[22] K. Seino, F. Bechstedt, and P. Kroll, Nanotechnology **20**, 135702 (2009).
[23] P. Dziawa, B. Taliashvili, W. Domuchowski, L. Kowalczyk, E. Lusakowska, A. Mycielski, V. Osinniy, and T. Story, Phys. Status Solidi C **2**, 1167 (2005).
[24] N. M. Ravindra, S. Auluck, and V. K. Srivastava, Phys. Status Solidi A **52**, K151 (1979).
[25] G. Nimtz, *Numerical Data and Functional Relationships in Science and Technology*, edited by O. Madelung, M. Schulz, and H. Weiss, Landolt-Börnstein, New Series, Group III, Vol. 17, (Springer, Berlin, 1983),.
[26] H. Preier, Appl. Phys. (Berlin) **20**, 189 (1979).
[27] K. Hannewald, S. Glutsch, and F. Bechstedt, Phys. Rev. B **62**, 4519 (2000).
[28] B. Adolph, V. I. Gavrilenko, K. Tenelsen, F. Bechstedt, and R. Del Sole, Phys. Rev. B **53**, 9797 (1996).
[29] R. W. Collins, M. A. Paesler, and W. Paul, Solid State Commun. **34**, 833 (1980).
[30] D. Engemann and R. Fischer, in *Amorphous and Liquid Semiconductors*, edited by R. A. Street, T. M. Searle, and I. G. Austin (Taylor and Francis, London, 1974).
[31] S. Sanguinetti, M. Henini, M. Grassi Alessi, M. Capizzi, P. Frigeri, and S. Franchi, Phys. Rev. B **60**, 8276 (1999).
[32] E. C. Le Ru, J. Fack, and R. Murray, Phys. Rev. B **67**, 245318 (2003).
[33] L. Brusaferri *et al.*, Appl. Phys. Lett. **69**, 3354 (1996).